

Gamma Knife radiosurgery of saccular aneurysms in a rabbit model

Mark D. Meadowcroft, PhD,^{1,2} Timothy K. Cooper, DVM, PhD, DACVP,^{3,4} Sebastian Rupprecht, BS,² Thaddeus C. Wright, BS,¹ Elizabeth E. Neely, BS,¹ Michele Ferenci, PhD,² Weimin Kang, PhD,¹ Qing X. Yang, PhD,^{1,2} Robert E. Harbaugh, MD,¹ James R. Connor, PhD,¹ and James McInerney, MD¹

Departments of ¹Neurosurgery, ²Radiology (The Center for NMR Research), ³Comparative Medicine, and ⁴Pathology, The Pennsylvania State University—College of Medicine, Milton S. Hershey Medical Center, Hershey, Pennsylvania

OBJECTIVE Intracranial aneurysms are vascular abnormalities associated with neurological morbidity and mortality due to risk of rupture. In addition, many aneurysm treatments have associated risk profiles that can preclude the prophylactic treatment of asymptomatic lesions. Gamma Knife radiosurgery (GKRS) is a standard treatment for trigeminal neuralgia, tumors, and arteriovenous malformations. Aneurysms associated with arteriovenous malformations have been noted to resolve after treatment of the malformation. The aim of this study was to determine the efficacy of GKRS treatment in a saccular aneurysm animal model.

METHODS Aneurysms were surgically produced using an elastase-induced aneurysm model in the right common carotid artery of 10 New Zealand white rabbits. Following initial observation for 4 years, each rabbit aneurysm was treated with a conformal GKRS isodose of 25 Gy to the 50% margin. Longitudinal MRI studies obtained over 2 years and terminal measures obtained at multiple time points were used to track aneurysm size and shape index modifications.

RESULTS Aneurysms did not rupture or involute during the observation period. Whole aneurysm and blood volume averages decreased with a linear trend, at rates of 1.7% and 1.6% per month, respectively, over 24 months. Aneurysm wall percent volume increased linearly at a rate of 0.3% per month, indicating a relative thickening of the aneurysm wall during occlusion. Nonsphericity of the average volume, aspect ratio, and isoperimetric ratio of whole aneurysm volume all remained constant. Histopathological samples demonstrated progressive reduction in aneurysm size and wall thickening, with subintimal fibrosis. Consistent shape indices demonstrate stable aneurysm patency and maintenance of minimal rupture risk following treatment.

CONCLUSIONS The data indicate that GKRS targeted to saccular aneurysms is associated with histopathological changes and linear reduction of aneurysm size over time. The results suggest that GKRS may be a viable, minimally invasive treatment option for intracranial aneurysm obliteration.

<https://thejns.org/doi/abs/10.3171/2017.6.JNS17722>

KEY WORDS aneurysm; Gamma Knife radiosurgery; GKRS; rabbit; saccular; vascular disorders; stereotactic radiosurgery

CEREBRAL saccular aneurysms account for 80%–90% of all intracranial aneurysms and are localized wall dilations that generally develop at arterial bifurcations. Roughly 6% (1 in 15) of individuals in the general population harbor these aneurysms. Rupturing of these vascular lesions leads to subarachnoid hemorrhagic stroke, with 50% mortality and morbidity rates.¹¹ Current treatment strategies include endovascular options of embolization (coiling or liquid) or flow diversion, and open surgical treatment, such as clipping or vascular bypass

procedures, all of which are invasive treatments with varying degrees of risk and effectiveness. Given these risks, asymptomatic aneurysms may not be appropriately treated prophylactically, and as a result, patients are not typically screened for intracranial aneurysms. Presently, there are no noninvasive treatment options for cerebral aneurysms. Current minimally invasive treatment for other cerebral vascular abnormalities, such as arteriovenous malformations (AVMs), include the use of Gamma Knife radiosurgery (GKRS), resulting in hemodynamic and histopatho-

ABBREVIATIONS AVM = arteriovenous malformation; GKRS = Gamma Knife radiosurgery; IPR = isoperimetric ratio; LCCA = left common carotid artery; NSI = nonsphericity index; RCCA = right common carotid artery; TOF = time of flight.

SUBMITTED March 21, 2017. **ACCEPTED** June 28, 2017.

INCLUDE WHEN CITING Published online January 12, 2018; DOI: 10.3171/2017.6.JNS17722.

logical alterations, with total obliteration over a period of 2–4 years.¹⁸ Gamma Knife radiosurgery is indicated for use as a treatment for a variety of neurological disorders; a dose of ionized radiation is focally administered deep within the brain, leaving the surrounding tissue largely unaffected. The GKRS treatment of AVMs with associated proximal cerebral aneurysms close to or within the nidus has resulted in complete obliteration of the AVM and aneurysms in 71% of cases.¹⁹ It is also known that endothelial cells exposed to gamma radiation in culture exhibit a fibrotic healing response;¹² this suggests a possible mechanism for GKRS-induced aneurysm obliteration.

The animal model in this study uses elastin degradation of the vessel walls, leading to progressive changes in the extracellular matrix and inflammatory infiltration that resembles naturally occurring cerebral saccular aneurysms. The resulting thin-walled aneurysms are morphologically and histologically similar, with hemodynamic pressure and shear stresses analogous to those of their human counterparts.³ Additionally, the size of the rabbit common carotid artery and modeled aneurysm is comparable to that of the human middle cerebral artery and the aneurysms that form there. The similarities to human cerebral aneurysms have established the elastase-induced model in the rabbit carotid artery as the gold standard by which to study saccular aneurysms.¹ The long-term patency of the rabbit aneurysm and the maintenance of dimensions without rupture for years following its creation further reiterate this principle.⁵

The purpose of this study was to test the hypothesis that GKRS treatment of saccular aneurysms will induce histopathological alterations of the aneurysm wall, leading to contraction and eventual occlusion. No previous study has investigated the effectiveness of GKRS treatment on aneurysm patency and obliteration rate. The use of GKRS for treating unruptured intracranial aneurysms, alone or in combination with endovascular treatment, could provide a minimally invasive, cost-effective, and promising addition to the treatment options available for intracranial aneurysms.

Methods

Localization of GKRS With Dosimetry Fiducial Phantom

An MRI-, CT-, and Gamma Knife-compatible cylindrical dosimetry phantom (outer diameter 76 mm, inner diameter 70 mm, length 145 mm) was created to test for parameter localization and dosimetric accuracy. A 10 × 10 × 2-mm optically stimulated luminescence medical dosimeter (nanoDot; Landauer, Inc.) was housed in a Delrin acetal resin cavity surrounded by fiducial water markers within the phantom. The phantom was placed within a rabbit holder built in-house that incorporated a bite bar, thermomesh with anchor points for immobilization, and a heating feature. The holder integrated a stereotactic coordinate head frame with a fiducial marker box (Elekta Instrument AB) for localization of imported MR/CT images and gamma radiation planning.

Experimental Animals and Aneurysm Generation

Eleven male New Zealand white rabbits (Robinson Services, Inc.; body weights 3–4 kg) were used in this study

design. All procedures were approved by the Institutional Animal Care and Use Committee at the Pennsylvania State University—Milton S. Hershey Medical Center and in accordance with the *Guide for the Care and Use of Laboratory Animals*.¹⁴ Elastase-induced saccular aneurysms were created in the right common carotid artery (RCCA) in accordance with previously described procedures.^{1,3,5} The rabbit aneurysm model has been described as the gold standard for simulating human intracranial aneurysms in terms of tortuosity and geometrical comparison.^{1,3}

In brief, approximately 30 minutes prior to anesthetic induction, subcutaneous injections of meloxicam (0.2 mg/kg), buprenorphine (0.05 mg/kg), and acepromazine (0.5 mg/kg), and intramuscular injections of enrofloxacin (15 mg/kg) (all drugs were drawn up in separate syringes) were administered. Anesthesia was induced with an intramuscular injection of ketamine (15 mg/kg) and dexmedetomidine (0.02 mg/kg) (combined in the same syringe). Animals were intubated, maintained on a breathing ventilator with 1.5% isoflurane, and placed on heating pads circulating warm air to maintain body temperature; their vital signs were continually monitored during surgery. With a sterile surgical technique, the RCCA was exposed and controlled with an underlayment pad, followed by temporary ligation to block blood flow with 4-0 silk proximally and distally. Papaverine (30 mg/ml) was directly administered as droplets from a 1-ml syringe onto the exposed RCCA to reduce vasospasm and maintain vascular tone.

A 5-Fr introducer sheath (AXcess 496005; Argon Medical Devices, Inc.) was inserted into the RCCA using the Seldinger technique and advanced retrograde, with the proximal point approximately 3 cm cephalad to the origin of the RCCA. The origin of the RCCA at the right subclavian and brachiocephalic artery junction was fluoroscopically determined (OEC 9800 Plus; General Electric Healthcare, Inc.) with retrograde injection of iodinated contrast media (Omnipaque 300-Iohexol; General Electric Healthcare, Inc.) through the introducer sidearm. A 4 × 7-mm balloon catheter (HyperForm; ev3 Endovascular, Inc.) was advanced through the introducer with fluoroscopic guidance to the level of the RCCA origin and inflated with contrast media to achieve flow arrest in the RCCA. A microcatheter and guidewire (Echelon 10 and X-Pedion 10; ev3 Endovascular, Inc.) were then inserted into the introducer, and the tip was placed approximately 5 mm from the inflated balloon with fluoroscopic guidance. Occlusion of the RCCA was verified with injection of contrast medium through the microcatheter, and a road map image was taken.

After verification of location of the microcatheter, 100 U (200 U/ml) porcine elastase (LS002290; Worthington Biochemical) was injected through the device and incubated within the lumen of the RCCA for 20 minutes. Following incubation, the RCCA was flushed with saline and back-bled to remove any remaining elastase. The RCCA was ligated with the proximal 4-0 silk suture approximately 12 mm from the origin of the RCCA below the catheter entry site. The distally placed 4-0 silk was used to ligate the RCCA so that no cranial back bleeding occurred through the catheterized artery. The surgical site was closed and sutured, and the animals were monitored dur-

ing recovery and given analgesic care. Aneurysms were allowed to mature over a period of 4 years, serving as an internal control in that they did not self-occlude over time. One animal died postsurgery due to complications, and another was killed at 48 months after aneurysm creation to act as a histological control for the GKRS-treated animals.

Magnetic Resonance Image Collection

Initial MR images of the 9 study animals were obtained 3 weeks after surgical aneurysm creation to demonstrate aneurysm formation. Prior to GKRS treatment, MR images of each rabbit were obtained using a 3-T MRI unit (Prisma; Siemens) at baseline, and then approximately every 3 months following GKRS for a 24-month period. Animals were anesthetized with intramuscular ketamine and xylazine (30 and 10 mg/kg, respectively, in the same syringe). Once sedated, both eyes were treated with ophthalmic ointment and a 24-gauge 3/4-inch intravenous catheter was placed in the marginal ear vein for administration of contrast agent and anesthetic reversal agent. Warming pads integrated into the animal holder were used to maintain the rabbits' body temperature. Following MRI, the anesthesia was reversed with 0.2 mg/kg yohimbine administered intravenously, and the rabbit was monitored until recovery. A T1-weighted 3D magnetization-prepared rapid-acquisition gradient echo data set was obtained with a matrix of $256 \times 256 \times 230$, field of view $25.6 \times 25.6 \times 23.0$ cm, 1 mm^3 isotropic resolution, TR 1500 msec, TE 2.34 msec, and 2 averages. A 3D time-of-flight (TOF) angiography data set was obtained with a matrix of $696 \times 768 \times 136$, field of view $16.3 \times 18.0 \times 9.5$ cm, $0.234 \times 0.234 \times 0.7$ -mm resolution, TR 23 msec, TE 3.78 msec, and 1 average. The 3D T1 and 3D TOF data sets were taken prior to and after administration of 0.1 ml/kg gadolinium enhancement (Gadavist; Bayer Healthcare Pharmaceuticals, Inc.) for pre- and postcontrast image sets.

GKRS Treatment

The 3D T1 and TOF MRI data sets were imported into the Gamma Knife planning workstation and were used to generate a 3D rendering of the rabbit head and neck region. The location of the aneurysm was determined and a gamma radiation dosing plan was created with one or two 4-mm spheres to cover the entirety of the aneurysm, including the neck (Fig. 1). A marginal dose of 25 Gy to the 50% isodose line was delivered with a Leksell Perfection system (Elekta AB). Oxygen saturation and respiration rate were monitored via camera from the viewing area outside the Gamma Knife control room with a pulse-oximeter machine.

Aneurysm Metric Acquisition and Measurement Criteria

Raw rabbit MRI DICOM files were imported and viewed with Aquarius iNtuition software (version 4.4.11.821.6784; TeraRecon). Measurements were taken in a semiblind fashion from the 3D TOF angiogram series obtained without contrast; the reviewers were blind to the animal and MRI time point. The z axis (height) was rotated to lie parallel to the plane of the aneurysm such that the cross section (x-y plane) would be in-plane with

the neck junction (RCCA-subclavian intersection). Using a polygon-measuring tool, both the exterior contour of the aneurysm and interior luminal cross-sectional areas were outlined manually. Whole aneurysm boundaries were determined by visually locating the aneurysm using all 3 planes of view, as well as the computer-generated 3D rendering (Fig. 2). The lumen area was measured at the edge of the brightest shade of gray within the whole aneurysm area. Output area, perimeter, and average diameter measurements were recorded for each image slice. Height was determined using the distance tool to measure the aneurysm from the neck to the end along the z axis.

Indices Classification

Indices for clinical interpretation of aneurysm shape were used to evaluate and characterize aneurysms over time.^{11,16} Shape indices of regularity have been shown to be effective predictors of rupture risk in aneurysms.⁹⁻¹¹ The indices evaluated are classified as zero order and are indicative of 3D nodal shape and size.

1D Size Indices

Three 1D size indices were defined as aneurysm height (H), which is the maximum perpendicular distance from each node to the neck boundary plane; maximum diameter (D_{max}), which is the maximum equivalent diameter for all cross sections that are parallel to the neck boundary plane; and neck diameter (D_n), which is the maximum diameter across the aneurysm neck boundary plane. To obtain D_{max} , a series of cutting planes parallel to the neck boundary plane were used to obtain consecutive cross sections of the aneurysm along its height. Because the neck boundary and cross sections are typically noncircular in shape, the definitions for D_{max} and D_n were drawn from the convention in fluid mechanics: $D = 4A/P$, where A is the area and P is the perimeter of the cross section.

2D Shape Indices

Three 2D shape indices were derived based on the 1D size measures: aspect ratio (AR), bottleneck factor (BF), and bulge location (BL). These were defined as follows: $AR = H/D_n$, $BF = D_{max}/D_n$, and $BL = H_b/H$, where H , D_n , and D_{max} are as defined above, and H_b is the distance of the largest cross section from the neck boundary plane.

3D Size Indices

With the aneurysm observable in n image slices, A_i and P_i are the area and perimeter, respectively, of an aneurysm in the i th image slice, and every adjacent MRI slice is equidistant. The 2 zero-order 3D size indices, volume (V) and surface area (S), are calculated using Riemannian type summation,¹⁷ as follows:

$$V = \frac{H}{n} \left(\frac{A_0}{2} + \sum_{i=1}^{n-1} A_i + \frac{A_n}{2} \right) \quad [\text{Eq. 1}]$$

$$S = \frac{H}{n} \left(\frac{P_0}{2} + \sum_{i=1}^{n-1} P_i + \frac{P_n}{2} \right) \quad [\text{Eq. 2}]$$

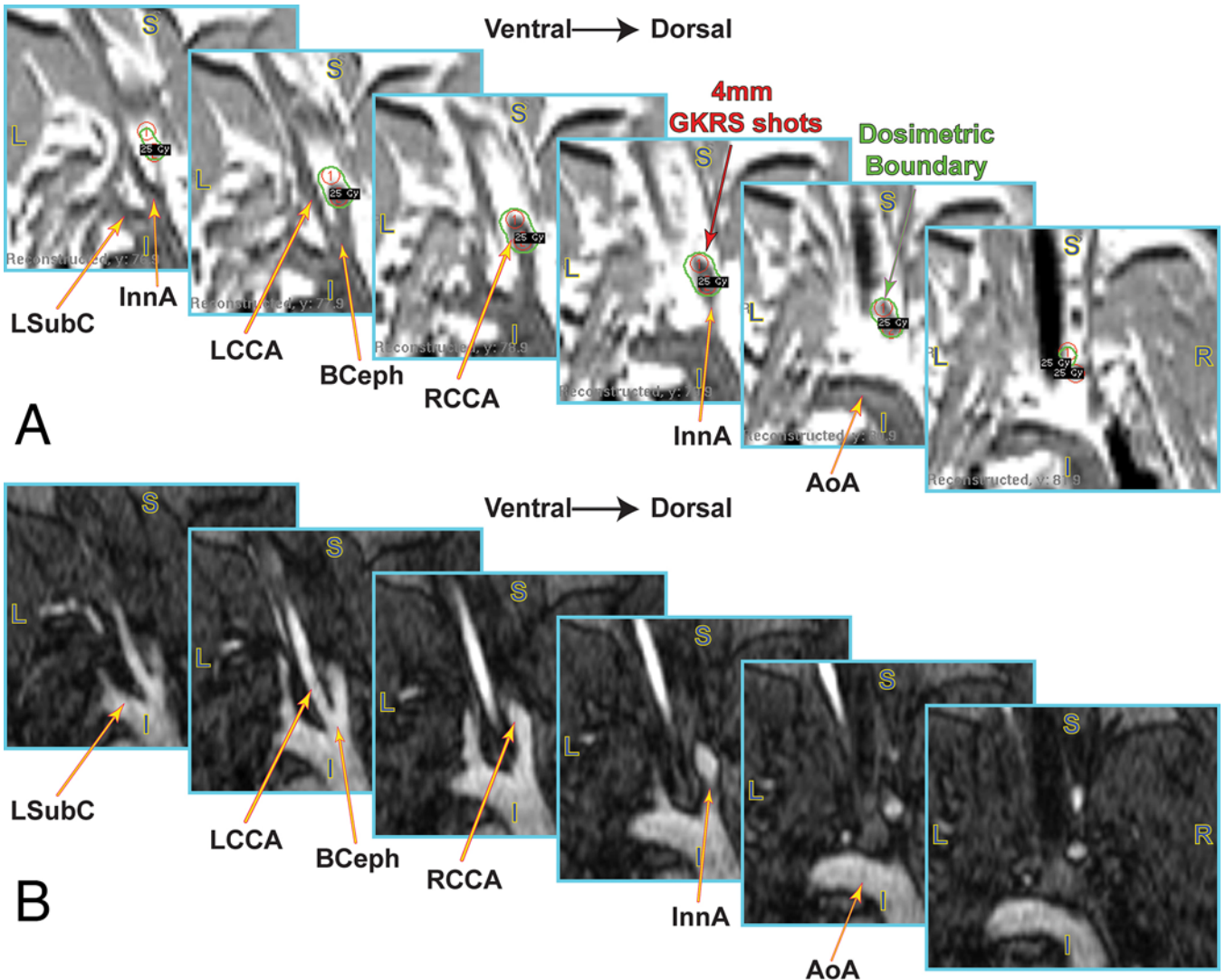


FIG. 1. Gamma radiation dosing plan (A) and TOF MR angiography (B) of the same slice selection. The left subclavian artery (LSubC), innominate artery (InnA), LCCA, brachiocephalic artery (BCeph), RCCA, and aortic arch (AoA) have yellow arrows indicating their location for orientation. A 25-Gy marginal dose to the 50% plan was localized with multiple 4-mm isodoses (red) from the neck region, branching from the BCeph to the entire aneurysm within the dosimetric boundary (green). Figure is available in color online only.

3D Shape Indices

The nonsphericity index (NSI) and isoperimetric ratio (IPR) are 3D shape indices based on volume and surface area, and are effective predictors of aneurysm rupture risk.^{11,16} The NSI describes how much deviation is shown by the aneurysm shape from a perfect sphere of equal-valued volume. The IPR is a nondimensionalized ratio of the surface area to the volume of a closed surface and represents a measure of the degree of folding of the surface.

The NSI and IPR are defined as follows:

$$NSI = 1 - \left((18\pi)^{\frac{1}{3}} \times \frac{V^{\frac{2}{3}}}{S} \right) \quad [\text{Eq. 3}]$$

$$IPR = \frac{S}{2V^{\frac{2}{3}}} \quad [\text{Eq. 4}]$$

Control Aneurysm Volume

Historical 2D rabbit aneurysm model data⁵ obtained over a period of 24 months were used to calculate the volume for comparison with data in this study. To model aneurysm volume with the historical 24-month data provided, it was assumed that the lesions were ellipsoid in shape with a spherical neck, such that volume was defined as follows:

$$V = \frac{\left(D_{max}^2 + \left(H + \frac{D_n}{2} \right) \pi \right)}{6} - \frac{\pi}{6} \times D_n^3 \quad [\text{Eq. 5}]$$

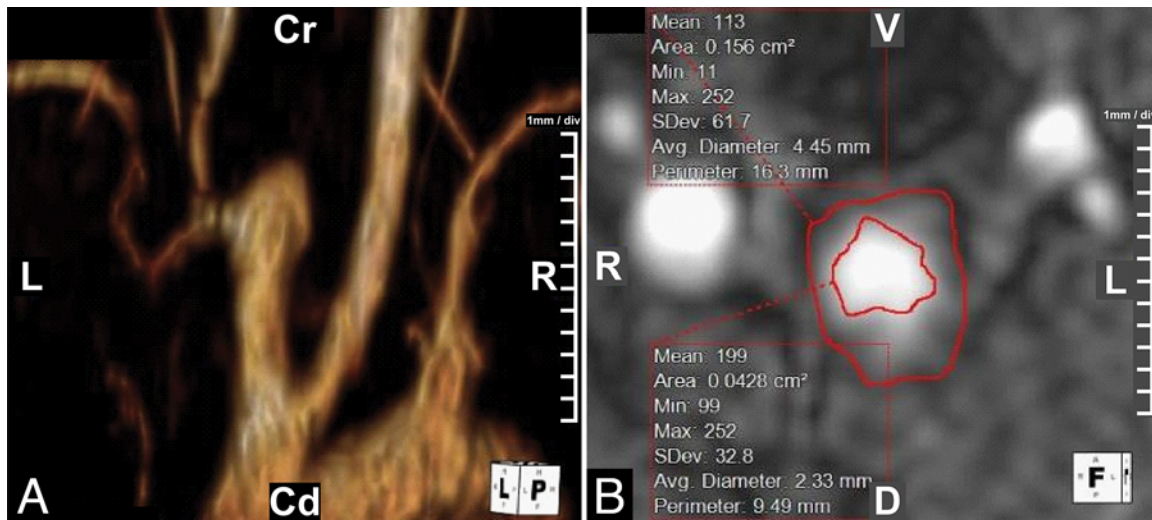


FIG. 2. A: A 3D rendering of the aneurysm TOF MRI data set in Fig. 1 at 2 months post-GKRS. B: Region of interest drawing done to obtain aneurysm volume and circumference measures from total and luminal blood. Cd = caudal; Cr = cranial; D = dorsal; V = ventral. Figure is available in color online only.

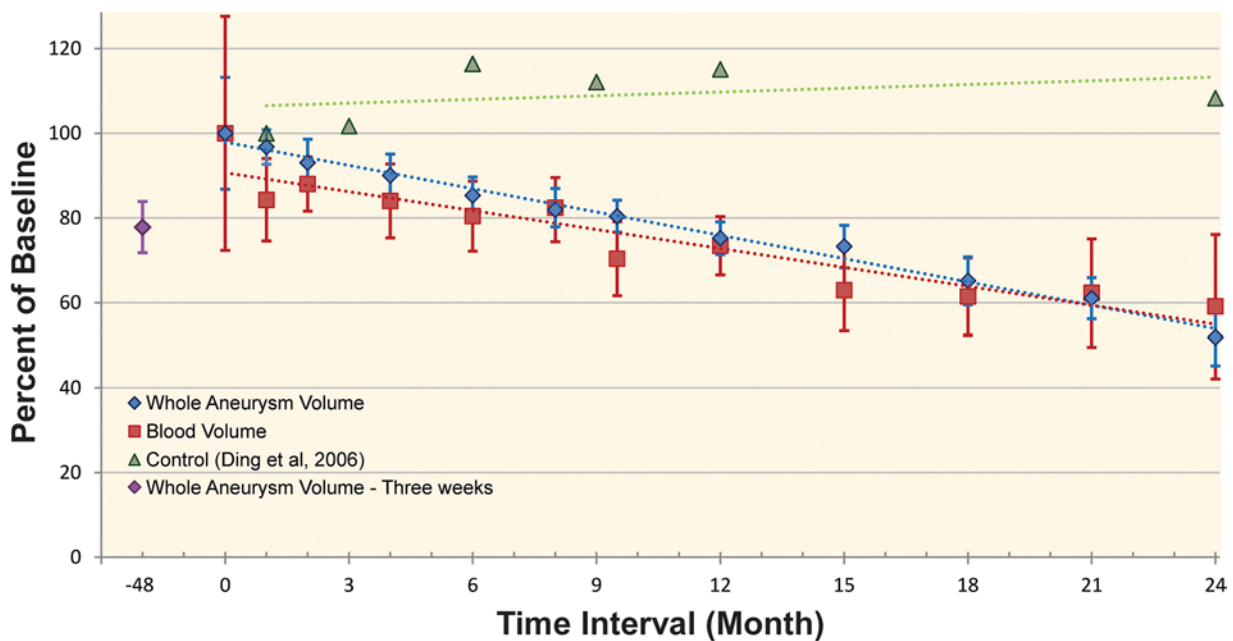


FIG. 3. Chart showing average percent change in whole aneurysm and luminal blood volume over 24 months with SEM. Control data are included from Ding et al. (2006) for reference. The experimental data indicate a linear decrease in both whole aneurysm (blue dotted line, $R^2 = 0.989$, $p < 0.001$) and luminal blood volume (red dotted line, $R^2 = 0.875$, $p < 0.001$) at a rate of -1.84% and -1.49% per month, respectively, for a total whole aneurysm and luminal volume decrease of 49% and 41% over 24 months. Historical control data (green dotted line) show a linear maintenance of volume over a 24-month period. The whole aneurysm volume at 3 weeks (purple diamond) was approximately 80% of the baseline size, indicating a volume increase to baseline at 48 months. Figure is available in color online only.

Carotid Artery Histology

Following euthanasia, the aortic arch with brachiocephalic trunk (innominate artery) and the RCCA and left common carotid artery (LCCA) to the cranial level of the angle of the mandible were dissected free and immersion fixed in 10% neutral buffered formalin. Sequential 2-mm cross sections were individually made from each carotid

artery and ordered in agarose.⁷ Samples were processed and embedded in paraffin, and sections were cut at a thickness of 6 μm . Tissue sections were stained with Masson's trichrome, Verhoeff van Gieson elastin, and Movat's pentachrome to visualize LCCA and RCCA histology.^{13,15} Slides were reviewed by an American College of Veterinary Pathologists diplomate pathologist, who was blinded

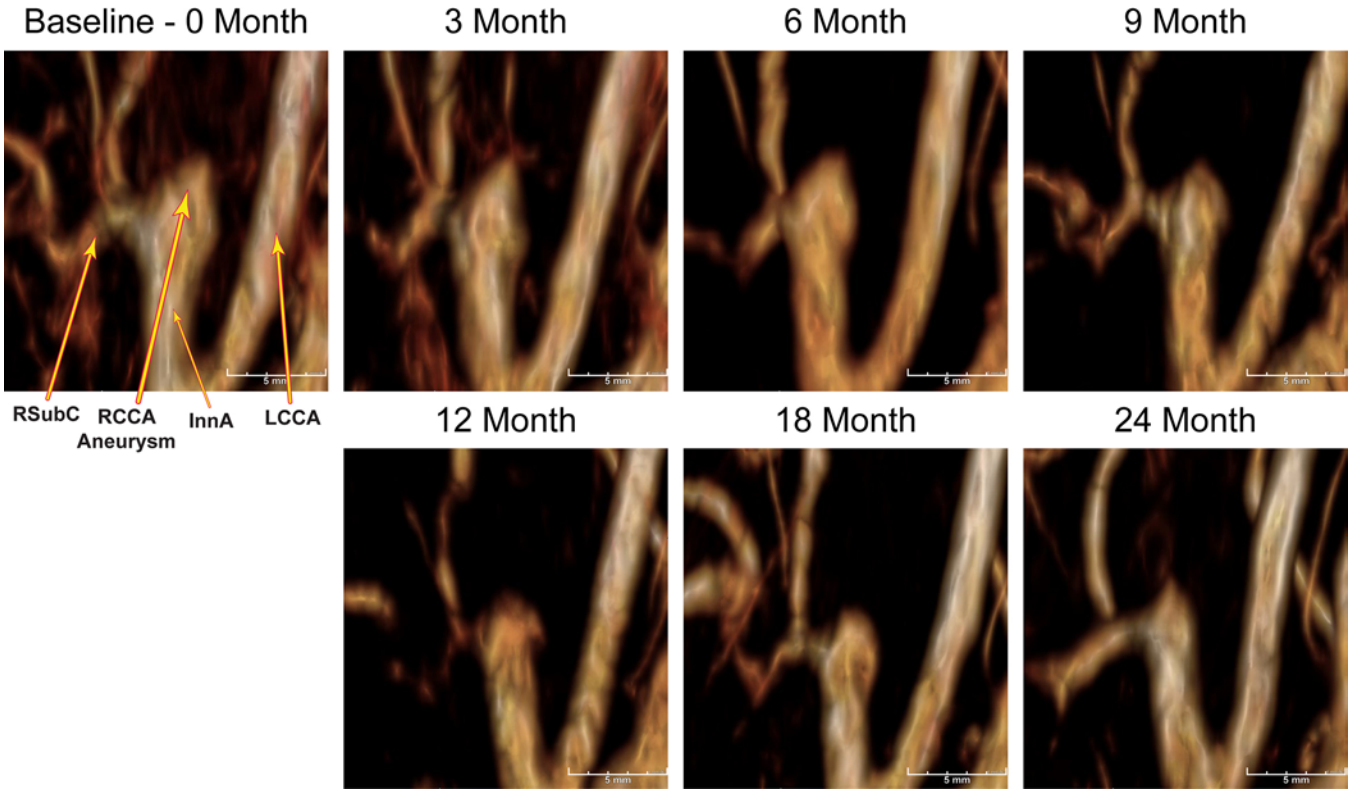


FIG. 4. A 3D rendering of TOF angiography data for the same aneurysm over 24 months. Image orientation and scale are maintained to aid in visualization. The right subclavian artery (RSubC), LCCA, innominate artery (InnA), and RCCA aneurysm are indicated for orientation. A gradual decline in whole aneurysm volume is visually seen over the study period, and mirrors the linear decrease in volume outlined in Fig. 3. Figure is available in color online only.

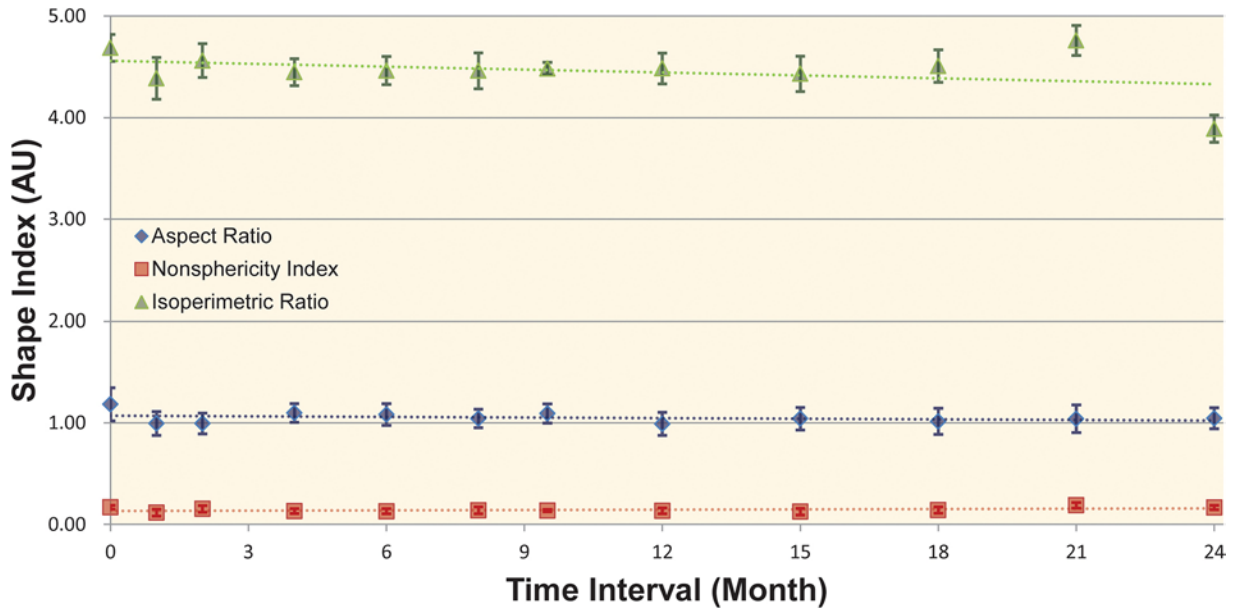


FIG. 5. Chart showing average shape indices, aspect ratio (blue), NSI (red), and IPR (green), over 24 months, with standard error. All aneurysm shape indices are maintained over the study period, indicating that rupture risk is static and not increasing. AU = arbitrary units. Figure is available in color online only.

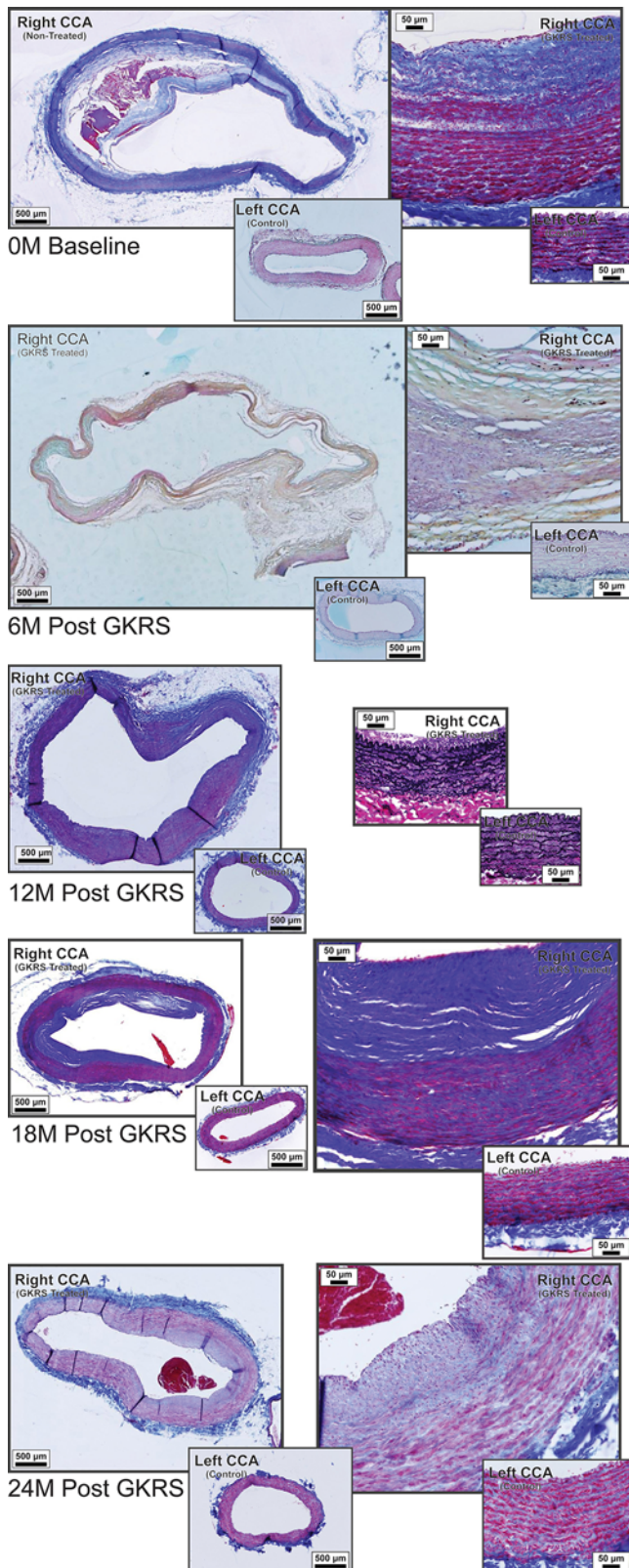


FIG. 6. Photomicrographs of tissues stained with Masson's trichrome (0 months), Verhoeff van Gieson elastin (12 months), and Movat's pentachrome (6 months). Samples of the RCCA aneurysms (large images) and LCCA controls (insets) obtained in representative rabbits over 24 months are shown. **FIG. 6.** (continued)→

FIG. 6. Whole RCCA aneurysm and control LCCA images (*left panel pairs*) have the same 500- μ m scale bar, and magnified images (*right panel pairs*) have the same 50- μ m scale bar. Visual inspection demonstrates intimal fibrosis with medial elastin fiber fragmentation and loss, with cystic medial degeneration at baseline and early following GKRS. Comparison of GKRS-treated aneurysms (RCCA) and untreated LCCAs demonstrates a gradual decline in aneurysm size, with subintimal and medial fibrotic thickening of the arterial wall. The size of the nontreated LCCA remains constant during treatment and over the 24-month period and demonstrates normal architecture with wall morphology consistent with advanced age, minimal to mild fibrosis, and mild to moderate elastolysis. Figure is available in color online only.

to intervention. All microscopic images and digital measurements were obtained with an Olympus BX51 microscope and DP71 digital camera by using cellSens Standard 1.12 imaging software (Olympus America).

Statistical Analysis

All statistical analyses were done with IBM SPSS version 24 (IBM Corp.). ANOVA with Tukey post hoc tests and Bonferroni correction were used to test significance across the longitudinal data such that $p < 0.05$ was considered significant.

Results

Phantom data indicate that localization and dosimetry of Gamma Knife radiation is accurate due to the integration of the stereotactic coordinate head frame with an MRI fiducial marker box into the animal holder. A single 4-mm-diameter, 8.6-Gy gamma radiation dose was localized and delivered to the center of the dosimeter phantom and was measured as 8.57 ± 0.008 Gy over 3 evaluations—demonstrating accurate localization and dosing of gamma radiation in the animal holder.

The 24-month data reveal a linear decline in total (blue, $R^2 = 0.989$, $p < 0.001$) and blood (red, $R^2 = 0.875$, $p < 0.001$) volume, with a rate of -1.84% and -1.49% per month, respectively (Fig. 3). Post hoc analysis determined that the percent of aneurysm total volume from baseline was significantly reduced at 9 months and onward ($p < 0.029$ to 0.001). Luminal blood volume was significantly different at 15 months and onward compared with baseline metrics ($p < 0.038$ to 0.001). The whole aneurysm and luminal volume linearly decreased approximately 45%–50% over the 2-year period. The whole aneurysm volume measurement 3 weeks after the initial aneurysm was approximately 80% that of baseline, demonstrating that aneurysm size increased slightly over the 48-month observation period before the baseline. Anatomical aneurysm volume visually decreases in a fashion similar to that of the whole aneurysm volume outlined previously (Fig. 4). The TOF angiography rendering approximately maintains a consistent view of the aneurysm and surrounding vasculature in the same animal over the 24-month period. All shape indices remained constant over the 24-month period (Fig. 5). The lack of change in the shape indices is demonstrative of overall aneurysm stability without an increase in rupture risk following GKRS.

Histological comparison of GKRS-treated aneurysms

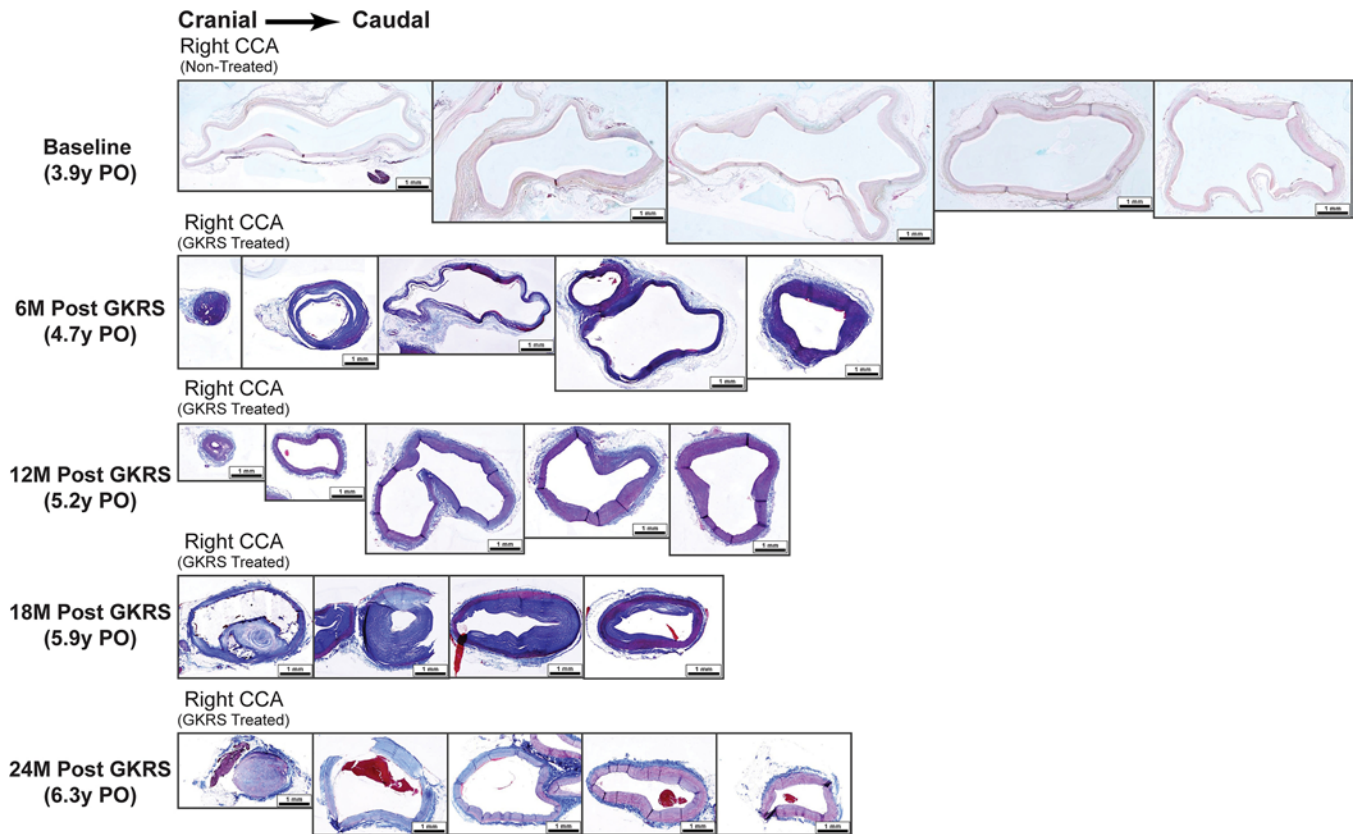


FIG. 7. Photomicrographs showing serial histological preparations along the cranial-to-caudal aneurysm axis over the 24-month period; all micrographs within are scaled to the same resolution (1-mm scale bar). Attenuation of the aneurysm wall with moderate to florid medial fibrosis occurs, becoming nearly circumferential, as seen over the 24-month period. Movat's pentachrome, baseline; Verhoeff van Gieson elastin, 6- and 18-month samples; and Masson's trichrome, 12- and 24-month samples. PO = postoperatively. Figure is available in color online only.

(in the RCCA) and untreated LCCAs demonstrates a gradual decline in aneurysm size, with subintimal and medial fibrotic thickening of the arterial wall (Figs. 6 and 7). All images have been scaled such that all gross micrographs maintain the same resolution to each other (500- μ m scale bar), as do the zoomed images (50- μ m scale bar). Serial histological samples of sections along the dorsal-to-ventral aneurysm axis are visualized in Fig. 7; all micrographs in that figure are scaled to the same resolution (1-mm scale bar). Baseline samples prepared at 0 months with Masson's trichrome demonstrate intimal fibrosis with medial elastin fiber fragmentation and loss, with cystic medial degeneration. Aneurysms at 6 months post-GKRS exhibit extensive intimal fibrosis at the cranial margin (Movat's pentachrome). Tissue at 12 months post-GKRS demonstrates moderate proliferative intimal lesions, with some recanalization of the right carotid artery cranial to the aneurysm (Verhoeff van Gieson stain for elastin). Histological investigation at 18 months post-GKRS demonstrates moderate circumferential wall expansion by extensive and florid mature, coarse, subintimal fibrosis lacking elastin, with mild medial fibrosis. Aneurysm tissue peripheral to the fibrosis has walls approaching that of regular tissue, with well-defined elastic fibers. The 24-month post-GKRS tissue demonstrates attenua-

tion (thickening) of the aneurysm wall, with moderate to florid medial fibrosis. The aneurysm is nearly circumferential, with medial elastolysis and fibrosis, subendothelial fibrin, few macrophages, and minimal nascent fibroplasia. The size of the nontreated LCCA remains constant during treatment and over the 24-month period, and demonstrates normal architecture, with wall morphology consistent with advanced age, minimal to mild fibrosis, and mild to moderate elastolysis.

The 2D measurements of the luminal, wall, and total areas illustrate a gradual decrease in lumen-to-total area ratio (Fig. 8A) and an increase in wall-to-total area ratio (Fig. 8B) over the 24-month period. These data are demonstrative of a gradual thickening of the aneurysm wall and a decrease in luminal volume over the 24-month period ($p < 0.01$), and closely mirror the MRI metrics over the same period (Figs. 3 and 4). Conversely, the lumen-to-total area and wall-to-total area ratios are maintained for the untreated LCCA control. The average lumen area demonstrates a decrease that is maintained throughout the 24-month period (Fig. 8C). The ratio of the RCCA (aneurysm) and LCCA lumen area demonstrates a decrease between the 6- and 12-month time points, echoing the previous lumen-to-wall area ratio and the average lumen area decrease ($p < 0.01$).

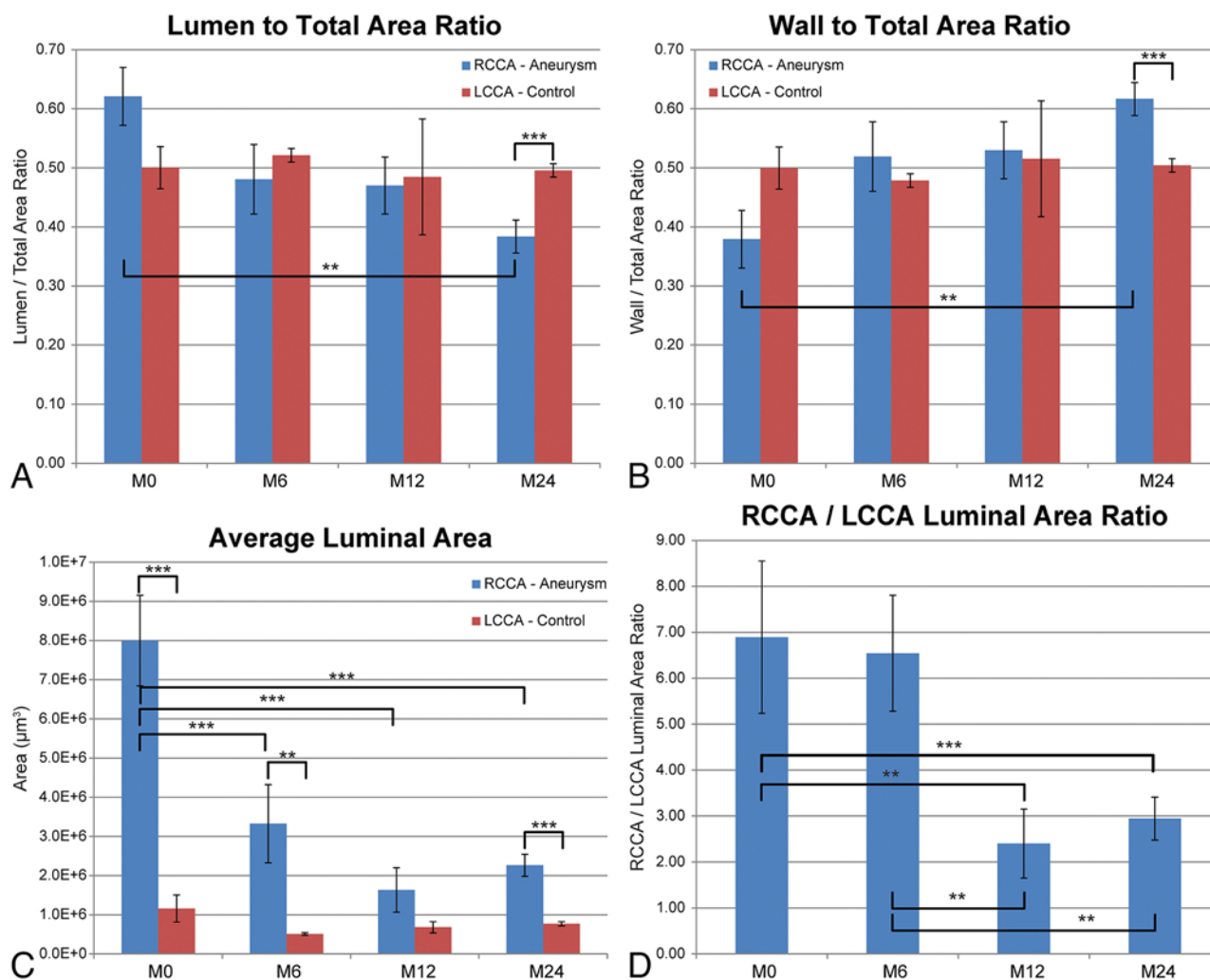


FIG. 8. Bar graphs showing the average 2D ratios and measurements of the luminal, wall, and total areas of aneurysms and LCCA control tissue. A gradual decrease in lumen-to-total area ratio (A) and an increase in wall-to-total area ratio (B) are demonstrated over the 24-month period, substantiating a gradual thickening of the aneurysm wall and decrease in luminal volume over the 24-month period. The data closely mirror the MRI metrics over the same period (see Figs. 3 and 4). Conversely, the lumen- and wall-to-total area ratios are maintained for the untreated LCCA control. The average lumen area demonstrates a decrease that is maintained throughout the 24-month period (C). The ratio of the RCCA (aneurysm) and LCCA luminal area demonstrates a decrease between the 6- and 12-month time points, echoing the previous lumen-to-wall and average lumen area decrease (D). M0, M6, M12, M24 = baseline, 6-month, 12-month, and 24-month measurements. ***p* < 0.01, ****p* < 0.001. Figure is available in color online only.

Discussion

The results of this work support the hypothesis that targeted GKRS treatment of saccular aneurysms results in histopathological improvement to the aneurysm wall and a reduction of aneurysm luminal volume without increasing rupture risk.

It has been reported that GKRS treatment of AVMs with coexistent aneurysms results in aneurysm volume reduction or obliteration.^{4,8,19} The mean latency interval between radiosurgery and AVM obliteration is approximately 24 months.¹⁹ However, the postradiosurgical response of a cerebral AVM is highly variable, with complete obliteration seen as early as a few months, as late as 5 years, or not at all during the follow-up period.^{2,6} The cause of obliteration of AVM-associated aneurysms has been speculated

to be related to reduction in blood flow and pressure, leading to adjacent feeding artery aneurysm obliteration. This high-flow hypothesis considers that reductions in AVM-associated blood flow and the pulsatile shear stress result in concomitant aneurysm disappearance. Having the aneurysm at the edge or outside of the radiosurgical plan has resulted in speculation that disappearance is related to hemodynamic changes rather than radiobiological factors.¹⁹ However, in other research the radiation dose is still considered to be present at the adjacent aneurysm, albeit to a lesser degree than at the centralized focal point.⁸ Whereas the main Gamma Knife dosage target of these studies was aimed at the AVM nidus, with the aneurysm situated outside the main radiation field,¹⁹ the mean marginal dosage received by AVM-associated aneurysms is calculated to

be on the order of 18 Gy.⁸ Our study used a small localized aneurysm dosage of 25 Gy at the 50% isodose, similar in strength to that focused on AVMs during radiosurgery over a much smaller volume.

The current data demonstrate that direct radiosurgical dosage centralized to the entire saccular aneurysm resulted in a 50% occlusion at 24 months. The period for complete aneurysm obliteration and/or occlusion with GKRS remains to be determined. Extrapolation of the linear longitudinal trend in the whole aneurysm and lumen volume tentatively suggests that complete occlusion could be realized in 48 months; however, the accuracy of this hypothesis requires further study. The volume reduction metrics and angiography renderings from the longitudinal MRI (Figs. 3 and 4, respectively) are reflected in the histological measures. Visual interpretation of the histological micrographs shows a decline in RCCA aneurysms' whole and luminal volume and fibrotic healing of the endovascular wall following GKRS over the 24-month period. A decrease in lumen-to-whole aneurysm ratio (Fig. 8A) and increase in wall-to-whole aneurysm ratio (Fig. 8B) parallel the MRI and micrograph data. Comparison of the untreated LCCA controls (Fig. 6 insets) demonstrates a static volume over the 2-year period (Fig. 8C); furthermore, the ratio of the RCCA/LCCA luminal volume (Fig. 8D) shows a decrease in luminal volume occurring between the 6- and 12-month time points.

Rupture risk associated with aneurysm radiosurgery is of primary concern, because it is unknown if wall thinning, loss of elastin, or endothelial scarring and/or hardening will occur following GKRS treatment. The constant trends observed in the 3 clinical shape indices (NSI, aspect ratio of average diameter, and IPR) indicate no increase of rupture risk following radiosurgery. Histological and MRI data support alterations in aneurysm centricity with wall thickening and volume decrease toward a more spheroid shape, which is generally considered to have a reduced rupture risk.^{11,16}

Although the outcome of this work demonstrates that aneurysm volume was reduced following GKRS, the data should be interpreted in the context of the study design and limitations. Of the study animals, 1 was used as an internal non-GKRS-treated control to visualize aneurysm histology at 48 months after aneurysm creation. Due to the preliminary nature of the work and the small number of animals used in the current study design, the possibility of having control animals for each time point in the study was not feasible. The historical control data provide an indication of the stability of these aneurysms over time. Additionally, the original MRI data obtained to verify aneurysm creation at 3 weeks, in comparison with the pre-GKRS MRI studies, demonstrate that aneurysms did not reduce naturally in size during the 4-year period. Due to the study design, it was not possible to completely blind evaluators, because all animals with MRI received GKRS. The evaluators who assessed the aneurysms were blind to the time point of the MRI for each animal.

Conclusions

Prior work has suggested that AVM-associated an-

eurysms that lie outside the GKRS high-dose AVM nidus treatment plan are sometimes obliterated because of hemodynamic changes following radiosurgery.¹⁹ Our data demonstrate that GKRS is successful in causing histopathological and hemodynamic changes in saccular aneurysms, linearly reducing the size of the aneurysm over time. Subsequent studies will aim to test the effects of the GKRS dose on a larger sample size over a longer period of time to assess the value of radiosensitizers in the use of GKRS as a minimally invasive treatment for saccular aneurysms.

Acknowledgments

Funding for this project has been made available by Elekta Instrument AB. We appreciate the contributions of balloon and microcatheters from Covidien/Medtronic in the pursuit of this research. We also appreciate the help of Maria Z. Chronos in the preparation of this manuscript.

References

- Altes TA, Cloft HJ, Short JG, DeGast A, Do HM, Helm GA, et al: 1999 ARRS Executive Council Award. Creation of saccular aneurysms in the rabbit: a model suitable for testing endovascular devices. *AJR Am J Roentgenol* **174**:349–354, 2000
- Blamek S, Tarnawski R, Miszczyk L: Linac-based stereotactic radiosurgery for brain arteriovenous malformations. *Clin Oncol (R Coll Radiol)* **23**:525–531, 2011
- Brinjikji W, Ding YH, Kallmes DF, Kadirvel R: From bench to bedside: utility of the rabbit elastase aneurysm model in preclinical studies of intracranial aneurysm treatment. *J Neurointerv Surg* **8**:521–525, 2016
- Ding D, Xu Z, Starke RM, Yen CP, Shih HH, Buell TJ, et al: Radiosurgery for cerebral arteriovenous malformations with associated arterial aneurysms. *World Neurosurg* **87**:77–90, 2016
- Ding YH, Dai D, Lewis DA, Danielson MA, Kadirvel R, Cloft HJ, et al: Long-term patency of elastase-induced aneurysm model in rabbits. *AJNR Am J Neuroradiol* **27**:139–141, 2006
- Fareed MM, Amro AA, Bayoumi Y, Orz YI, Tunio M, Maklad A, et al: LINAC stereotactic radiosurgery for brain arteriovenous malformation: a single institutional experience from Saudi Arabia. *Neurosci Discov* **1**:1, 2013
- Habashi JP, Judge DP, Holm TM, Cohn RD, Loeys BL, Cooper TK, et al: Losartan, an AT1 antagonist, prevents aortic aneurysm in a mouse model of Marfan syndrome. *Science* **312**:117–121, 2006
- Kim M, Pyo S, Jeong Y, Lee S, Jung Y, Jeong H: Gamma Knife surgery for intracranial aneurysms associated with arteriovenous malformations. *J Neurosurg* **105 Suppl**:229–234, 2006
- Kleinloog R, de Mul N, Verweij BH, Post JA, Rinkel GJE, Ruijgrok YM: Risk factors for intracranial aneurysm rupture: a systematic review. *Neurosurgery* [epub ahead of print], 2017
- Lindgren AE, Koivisto T, Björkman J, von Und Zu Fraunberg M, Helin K, Jääskeläinen JE, et al: Irregular shape of intracranial aneurysm indicates rupture risk irrespective of size in a population-based cohort. *Stroke* **47**:1219–1226, 2016
- Ma B, Harbaugh RE, Raghavan ML: Three-dimensional geometrical characterization of cerebral aneurysms. *Ann Biomed Eng* **32**:264–273, 2004

12. Mothersill C, Seymour CB, Mulvin D, Hennessy TP: Endothelial cell proliferation is induced by radiation in cultured explants of human urothelium and oesophageal mucosa. **EXS** **61**:407–410, 1992
13. Movat HZ: Demonstration of all connective tissue elements in a single section; pentachrome stains. **AMA Arch Pathol** **60**:289–295, 1955
14. National Research Council: **Guide for the Care and Use of Laboratory Animals**, ed 8. Washington, DC: National Academies Press, 2011 (<https://www.ncbi.nlm.nih.gov/books/NBK54050/>) [Accessed August 31, 2017]
15. Prophet EB, Mills B, Arrington JB, Sobin LH (eds): **Laboratory Methods in Histotechnology**. Washington, DC: American Registry of Pathology, 1992
16. Raghavan ML, Ma B, Harbaugh RE: Quantified aneurysm shape and rupture risk. **J Neurosurg** **102**:355–362, 2005
17. Riemann B, Wilkins DR: **Grundlagen für eine allgemeine Theorie der Functionen einer veränderlichen complexen Grösse**. Göttingen: EA Huth, 1851
18. Schneider BF, Eberhard DA, Steiner LE: Histopathology of arteriovenous malformations after gamma knife radiosurgery. **J Neurosurg** **87**:352–357, 1997
19. Vymazal J, Liscák R, Novotný J Jr, Janousková L, Vladyka V: The role of Gamma Knife radiosurgery in arteriovenous

malformation with aneurysms. **Stereotact Funct Neurosurg** **72 (Suppl 1)**:175–184, 1999

Disclosures

Dr. McInerney received clinical or research support for the study described (includes equipment or material) from Elekta.

Author Contributions

Conception and design: Meadowcroft, Yang, Harbaugh, Connor, McInerney. Acquisition of data: Meadowcroft, Cooper, Rupprecht, Neely, Ferenci, Kang. Analysis and interpretation of data: Meadowcroft, Wright, Yang. Drafting the article: Meadowcroft. Critically revising the article: Meadowcroft, Cooper, Yang, Harbaugh, Connor, McInerney. Reviewed submitted version of manuscript: Meadowcroft, Cooper, McInerney. Approved the final version of the manuscript on behalf of all authors: Meadowcroft. Statistical analysis: Meadowcroft. Administrative/technical/material support: Meadowcroft. Study supervision: Meadowcroft, McInerney.

Correspondence

Mark D. Meadowcroft: Milton S. Hershey Medical Center, Center for NMR Research, Hershey, PA. markmeadowcroft@psu.edu.